Controlling the Localization of Polymer-Functionalized Nanoparticles in Mixed Lipid/Polymer Membranes

Adekunle Olubummo,[†,⊥] Matthias Schulz,[†,⊥] Bob-Dan Lechner,[‡] Peggy Scholtysek,[‡] Kirsten Bacia,[§] Alfred Blume,[‡] Jörg Kressler,[‡] and Wolfgang H. Binder[†,*]

[†]Macromolecular Chemistry, Institute of Chemistry, Faculty of Natural Sciences II (Chemistry, Physics and Mathematics), Martin-Luther University Halle—Wittenberg, D-06120 Halle (Saale), Germany, [‡]Physical Chemistry, Institute of Chemistry, Faculty of Natural Sciences II (Chemistry, Physics and Mathematics), Martin-Luther University Halle—Wittenberg, D-06120 Halle (Saale), Germany, and [§]ZIK HALOmem, Martin-Luther University Halle—Wittenberg, D-06120 Halle (Saale), Germany. [⊥]A.O. and M.S. contributed equally to this article.

ABSTRACT Surface hydrophobicity plays a significant role in controlling the interactions between nanoparticles and lipid membranes. In principle, a nanoparticle can be encapsulated into a liposome, either being incorporated into the hydrophobic bilayer interior or trapped within the aqueous vesicle core. In this paper, we demonstrate the preparation and characterization of polymer-functionalized CdSe NPs, tuning their interaction with mixed lipid/polymer membranes from 1,2-dipalmitoyl-*sn*-glycero-3-phophocholine and PIB_{87}-*b*-PEO_{17} block copolymer by varying their surface hydrophobicity. It is observed that hydrophobic PIB-modified CdSe NPs can be selectively located within polymer domains in a mixed lipid/polymer monolayer at the air/water interface, changing their typical domain morphologies, while amphiphilic PIB-PEO-modified CdSe NPs showed no specific localization in phase-separated lipid/polymer films. In addition, hydrophilic water-soluble CdSe NPs can readily adsorb onto spread monolayers, showing a larger effect on the molecule packing at the air/water interface in the case of pure lipid films compared to mixed monolayers. Furthermore, the incorporation of PIB-modified CdSe NPs into hybrid lipid/polymer GUVs is demonstrated with respect to the prevailing phase state of the hybrid membrane. Monitoring fluorescent-labeled PIB-CdSe NPs embedded into phase-separated vesicles, it is demonstrated that they are enriched in one specific phase, thus probing their selective incorporation into the hydrophobic portion of PIB_{87}-*b*-PEO_{17} BCP-rich domains. Thus, the formation of biocompatible hybrid GUVs with selectively incorporated nanoparticles opens a new perspective for subtle engineering of membranes together with their (nano-) phase structure serving as a model system in designing functional nanomaterials for effective nanomedicine or drug delivery.

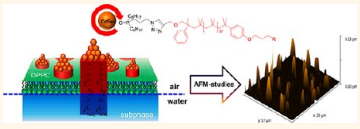

KEYWORDS: nanoparticles · mixed lipid/polymer membrane · diblock copolymer · localization · hydrophobicity · hybrid GUVs · selective incorporation

Research in understanding the interaction between functional surface-modified nanoparticles with lipid or polymer membranes has grown significantly over the past years,[1−3] aiming to use nanoparticle/lipid hybrid systems for broad biomedical applications and nanotechnology and as therapeutic agents with minimal cytotoxicity. These applications can be achieved only with a tailored control over nanoparticles' interaction with lipid or polymer membranes. Thus, the nanoparticles' surface chemistry plays an important role together with other unique nanoparticle properties such as size, shape, surface charge, and chemical composition.[1,4−7]

Both vesicular lipid membranes (liposomes[8]) and polymer membranes (polymersomes[9]) feature a membrane bilayer that differentiates the hydrophilic properties inside their aqueous cavity from the hydrophobic properties within their bilayer interior.[10] This clear-cut difference provides possibilities of selective location, dispersing or concentration of nanoparticles *via* encapsulation, binding, or specific interfacial interactions. Liposomes are a construct of naturally occurring phospholipids with low molecular weight, whereas polymersomes in contrast are constructed solely from amphiphilic diblock copolymers with a molecular weight up to 100 kg/mol, thus offering a chance to tune the dimensions as well as the chemical properties of the membrane. As a result, polymersomes show a higher mechanical and thermal stability within their curved membrane and have thus gained significant use in biomedical applications.[9,11,12]

Hydrophobicity[13,14] in particular plays a very important role when dealing with the interaction between NPs and liposomes, as nanoparticle assembly and lipid stabilization are essentially driven by hydrophobic/hydrophilic (interfacial) effects,[15] entrapping nanoparticles within the aqueous vesicle core or into the hydrophobic part of the lipid bilayer. Embedding functional hydrophobic nanoparticles provides a plethora of different applications for controlling bilayer permeability, biocompatibility, and liposomal

* Address correspondence to wolfgang.binder@chemie.uni-halle.de.

Received for review May 29, 2012 and accepted September 5, 2012.

Published online September 05, 2012
10.1021/nn3023602

release, also useful for investigating biochemical reactions *in vitro*. In order to embed NPs into the hydrophobic membrane interior of a lipid bilayer, the nanoparticle must fulfill two requirements: first, it must be small enough (diameter less than 8 nm) to fit within the lipid bilayer dimension (~4 nm), and second, it must possess a hydrophobic surface. Thus, a plethora of hydrophobic nanoparticles such as fullerene (C_{60}),[16,17] gold,[1,18] silver,[19,20] SiO_2,[21] and quantum dots[2,22–24] have been comfortably embedded within lipid bilayers without significantly compromising the liposome structure. The enrichment of surface-functionalized hydrophobic nanoparticles within the lipid bilayer interior has been explained by Korgel *et al.*[25] as a result of NP interaction with the hydrophobic tail of the lipid molecules. Thus, hydrophobic nanoparticles can cause the bilayer to "unzip" when they are located at the center, leading to changes in lipid packing and disruption of lipid–lipid interactions between the lipid head groups and/or the lipid alkyl tails. This unzipping creates void space around the nanoparticles, resulting in nanoparticle clustering and minimization of the free energy of deformation. The incorporation of nanoparticles forming a hydrophobic or hydrophilic shell has been further reported in the literature to induce some secondary effects such as reduced lipid ordering with increasing nanoparticle loading,[26] formation of holes,[27] curving effects to or from the membrane,[28,29] and fission and budding of vesicles.[30]

The interaction of surface-functionalized nanoparticles with block copolymer (BCP) vesicles (polymersomes) has been shown to offer a convenient way of controlling the arrangement of nanoparticles in polymer vesicles by segregating nanoparticles into a more favorable interacting polymer domain or at the interface between two polymers.[31,5] Polymer–nanoparticle interactions can induce a morphological change of block copolymer assemblies,[32,33] thus enabling the segregation of the NPs into the central hydrophobic position of either the membrane or its interface.[34] Eisenberg *et al.*[35] have shown that nanoparticles can selectively be incorporated into the central portion of block copolymer vesicle walls by coating the particles with a diblock copolymer having a similar structure to that of the diblock copolymers used in forming the polymersomal membrane. This allows the particles to be preferentially localized in the central portion of the membrane wall. The localization of surface-functionalized nanoparticles into a specific portion of the polymersomal membrane has also been shown to induce vesicle aggregation.[36,37]

Recently, we have demonstrated the formation of truly biocompatible hybrid mono- and bilayer membranes[38] composed of an amphiphilic PIB_{87}-*b*-PEO_{17} BCP (PIB = poly(isobutylene); PEO = poly(ethylene oxide)) and a natural lipid (1,2-dipalmitoyl-*sn*-glycero-3-phophocholine, DPPC). In general, the incorporation of such amphiphilic polymers into lipid membranes has been shown to influence transport properties, membrane stability and curvature and that they induce channels in the lipid membranes.[6,39] Only a few examples[40–43] have been reported in the literature until now demonstrating a mixture between amphiphilic block copolymers and biological phospholipids within a bilayer membrane. It was observed that the incorporation of biocompatible polymers into DPPC monolayers using different amphiphilic PIB-PEO BCPs to DPPC ratios leads to remarkable effects on the lipid bilayer organization (*i.e.*, the formation of a demixed system forming lipid- and polymer-rich domains from 20 to 28 mol % of the diblock copolymer). Thus, we were interested in investigating the selective localization of hydrophobic/hydrophilic surface-functionalized nanoparticles in this demixed system, which may open a new prospective for subtle engineering of membranes and their nanoporosity, nanophased structure, and mechanical properties, serving as a model system in designing functional nanomaterials for effective nanomedicine or drug delivery.

In the present paper, we report the synthesis of polymer-grafted, hydrophobic, hydrophilic, and amphiphilic surface-functionalized CdSe NPs aiming at controlling their selective localization in a binary lipid/polymer mixture *via* a direct assembly method on a Langmuir monolayer (see Figure 1). As the now controllable interaction between the nanoparticle surfaces and the lipid/polymer part should allow a selective location, the synthesis of appropriately surface-functionalized nanoparticles with grafted polymer chains was envisioned. In order to further investigate the nanoparticle location within the monolayer, atomic force microscopy (AFM) and fluorescence monolayer studies were performed, also probing the selective interaction of the water-soluble hydrophilic NPs in the binary mixed system *via* adsorption measurements. The selective interaction between functionalized NPs and polymer domains in mixed monolayers can enhance the incorporation and localization of hydrophobic NPs into hybrid bilayer membranes. Furthermore, we were able to demonstrate the selective incorporation of PIB-modified CdSe NPs into the BCP phase of the phase-separated hybrid bilayer membrane composed of DPPC and the PIB_{87}-*b*-PEO_{17} BCP.

RESULT AND DISCUSSION

As part of the concept to investigate the controlled nanoparticle location in mixed lipid/polymer membranes, different nanoparticles with grafted polymer chains were investigated, featuring either purely hydrophobic, purely hydrophilic, or amphiphilic surface properties. As quantum dots can be prepared easily and their ligand exchange has been investigated intensely, CdSe nanoparticles (sized ~2 nm) were chosen as inorganic cores, together with phosphine oxides as ligands binding tightly but still exchangeable

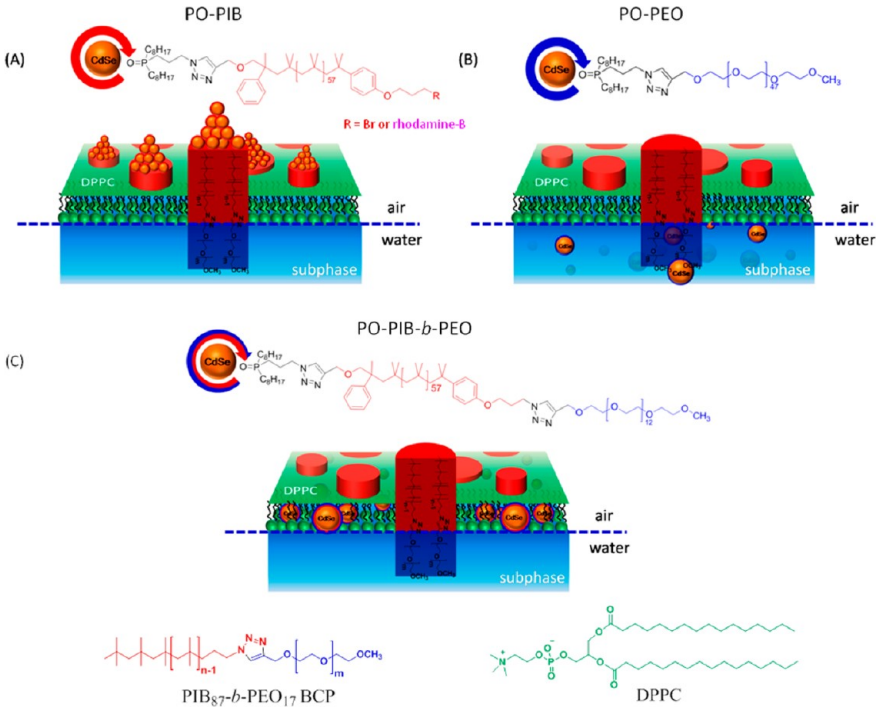

Figure 1. General concept for the location of polymer-functionalized CdSe nanoparticles in mixed DPPC/PIB_{87}-*b*-PEO_{17} BCP monolayers. (A) Specific location of hydrophobically modified NPs on top of the polymer domains, (B) interaction of water-soluble NPs with mixed lipid/polymer monolayers within the subphase, and (C) unspecific location of amphiphilic NPs in mixed monolayers at the air/water interface.

onto the quantum-dot surface. With poly(isobutylene) as hydrophobic and poly(ethylene oxide) as hydrophilic polymer a simple methodology of generating all three types of nanoparticles can be executed, using block copolymers composed of PIB-PEO in the case of amphiphilic nanoparticles. The following parts describe the synthesis of such polymer-covered quantum dots, as well as their interaction with lipid monolayers in different, mixed, or phase-separated conditions.

Synthesis of Polymer-Functionalized CdSe NPs. CdSe NPs, covered with either hydrophobic PIB_{57} (**NP3**), hydrophilic PEO_{47} (**NP4**), or the amphiphilic block copolymer PIB_{57}-*b*-PEO_{12} (**NP5**) were synthesized by exchanging the passivating trioctylphosphine oxide (TOPO) on **NP1** with a weak bonding pyridine to furnish **NP2**, followed by ligand exchange with either α-phosphineoxide-γ-bromo telechelic PIB ($M_{n(GPC)}$ = 3200 g/mol; M_w/M_n = 1.3) (**1**), α-phosphineoxide-γ-methylene telechelic PEO ($M_{n(GPC)}$ = 2100 g/mol, M_w/M_n = 1.2) (**3**), or α-phosphineoxide-γ-poly(ethylene oxide) telechelic polyisobutylene ($M_{n(GPC)}$ = 3560 g/mol; M_w/M_n = 1.3) (**4**),[44] yielding polymer-functionalized nanoparticles **NP3**, **NP4**, and **NP5**, respectively (see Scheme 1 and Scheme 2). All polymers were prepared *via* living polymerization methods, thus ensuring low polydispersity and controlled molecular weights, and subsequently attached to the nanoparticles *via* the phosphine oxide ligand as explained in the literature,[44] forming a highly stable bond. UV−vis measurements of the TOPO (**NP1**) and polymer-covered nanoparticles (**NP3**, **NP4**, and **NP5**) were conducted to ensure that no oxidation or aggregation had taken place during the pyridine treatment[45] (see Supporting Information Figure S1). According to the size and wavelength equation proposed by Peng *et al.*,[46] the first exciton peak at 512 nm corresponds to a 2.4 nm core diameter of the nanoparticles. After ligand exchange with polymers **1**, **3**, and **4**, the first exciton peak of **NP1** still remained at around 512 nm, indicating the absence of aggregation or oxidation of the NPs during the process of ligand exchange. NMR spectroscopy showed that the signals coming from the part of the ligands being in the direct neighborhood or bound to the NP surface were strongly broadened or shifted in comparison to the free unbounded ligand. This can especially be observed in the broadening of the proton peak at 1.6−2.2 ppm in the phosphine oxide ligand bound to the NP surface (see Supporting Information Figure S2), which is in agreement with literature values.[47−49] The IR spectrum of **NP3**, **NP4**, and **NP5** showed peaks matching all the polymer peaks in frequency and relative intensity, except for the P−O stretching vibration in the region 1200−900 cm^{-1}, which is shifted about 20 cm^{-1} and broadened, confirming the direct attachment of the polymer to the NP surface (see Supporting Information Figure S5). These results are in good agreement with IR measurements performed on triphenylphosphine oxide ligand complexing to CdI_2 and other metal salts,[50] which typically show a shift in the P−O vibrational frequency between 20 and 60 cm^{-1} upon complexation.

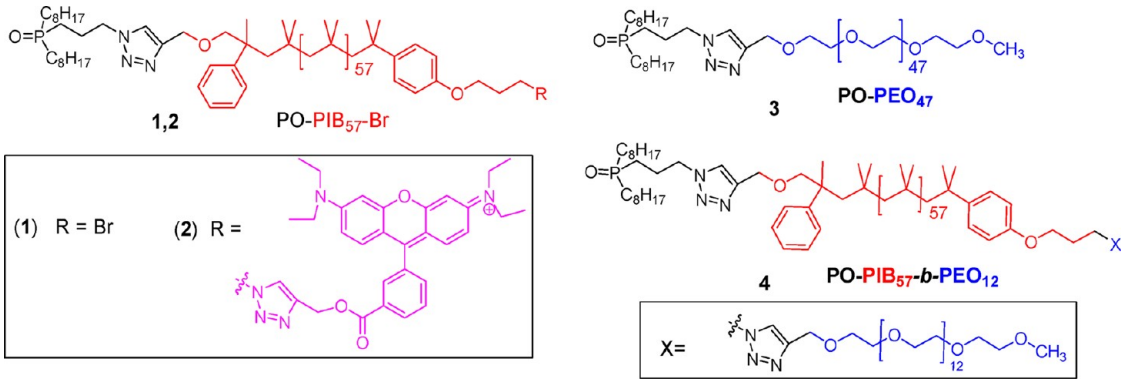

Scheme 1. Phosphine oxide (PO) ligands 1−4 used for the nanoparticle functionalization.

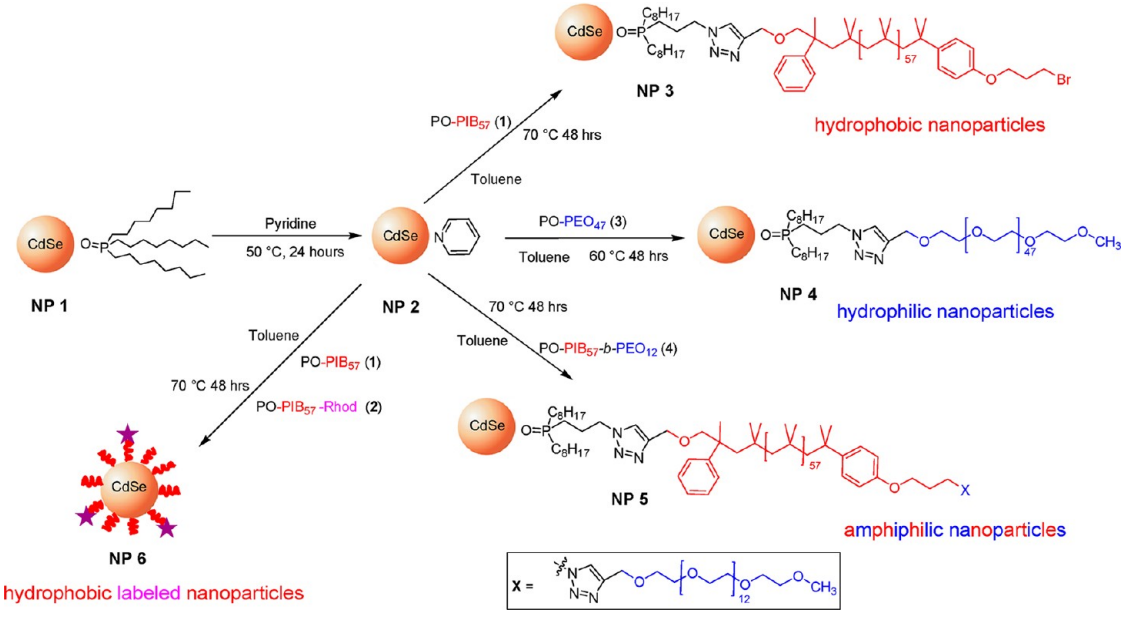

Scheme 2. Synthesis of polymer-functionalized CdSe nanoparticles.

The change in size of the nanoparticles as a result of replacing the TOPO ligand in **NP1** with the polymer **1**, **3**, or **4** was monitored by dynamic light scattering (DLS), which shows that replacing TOPO with α-phosphineoxide-γ-bromotelechelic PIB (PO-PIB_{56}-Br) (**1**), α-phosphineoxide-γ-methylene telechelic PEO (PO-PEO_{47}) (**3**), or α-phosphineoxide-γ-polyethylene oxide telechelic PO-PIB_{57}-PEO_{12} (**4**) induced an increase in the hydrodynamic diameter from 2.4 nm to 6.4 nm for the hydrophobic PO-PIB_{56}-Br-covered CdSe-NPs (**NP3**), to 9.9 nm for the hydrophilic PO-PEO_{47}-covered CdSe NPs (**NP4**), and to about 11 nm for the amphiphilic PO-PIB_{57}-*b*-PEO_{12} (**NP5**) (see Table 1).

Thermogravimetric (TGA) measurements were conducted to evaluate the amount of polymer chains attached to the nanoparticles' surface. Thus, the grafting density of chains was obtained by relating the weight loss to the NP surface area using equation S1 according to ref 51 (see Supporting Information), resulting in a grafting density of 0.5 chains/nm^2 for the hydrophobic PIB_{57}-covered CdSe nanoparticles (**NP3**), 0.47 chains/nm^2 for the hydrophilic PEO_{47}-covered CdSe NPs (**NP4**), and 0.53 chains/nm^2 for the amphiphilic PO-PIB_{57}-PEO_{12}-covered nanoparticles (**NP5**).

According to UV−vis measurements, we calculated an average of three chains of rhodamine-B-labeled PIB (**2**) were attached to each nanoparticle, furnishing the fluorescent-labeled **NP6**. The UV−vis intensity at a known concentration of rhodamine-B-labeled PIB (**2**) was compared with that of a known concentration of the labeled **NP6**. As the amount of NPs at this concentration is known, the amount of polymer equaling the number of polymer chains attached to each nanoparticle was easily determined (see Supporting Information Figure S10).

Interaction and Location of Hydrophobic CdSe NPs (NP3) in Hybrid Monolayers. Effects of differently surface-modified NPs (**NP3** and **NP5**) on the phase behavior of mixed DPPC:PIB_{87}-*b*-PEO_{17} monolayers were extensively studied by Langmuir monolayer measurements, serving as a model for half a bilayer membrane.

TABLE 1. Characterization Data for NP3, NP4, NP5, and NP6 *via* DLS, TGA, and UV−Vis and Fluorescence Spectroscopy

NP	size before ligand exchange (nm)	size after ligand exchange (nm)[a]	grafting density (chains/nm^2)[b]	absorption maximum after ligand exchange (nm)[c]	emission maximum after ligand exchange (nm)[c]
NP3	2.4	6.4	0.5	513	625
NP4	2.4	9.9	0.47	513	570
NP5	2.4	11	0.53	513	540
NP6	2.4	6.3	0.52	513	585

[a] Determined by DLS. [b] Determined by TGA. [c] Determined by fluorescence spectroscopy.

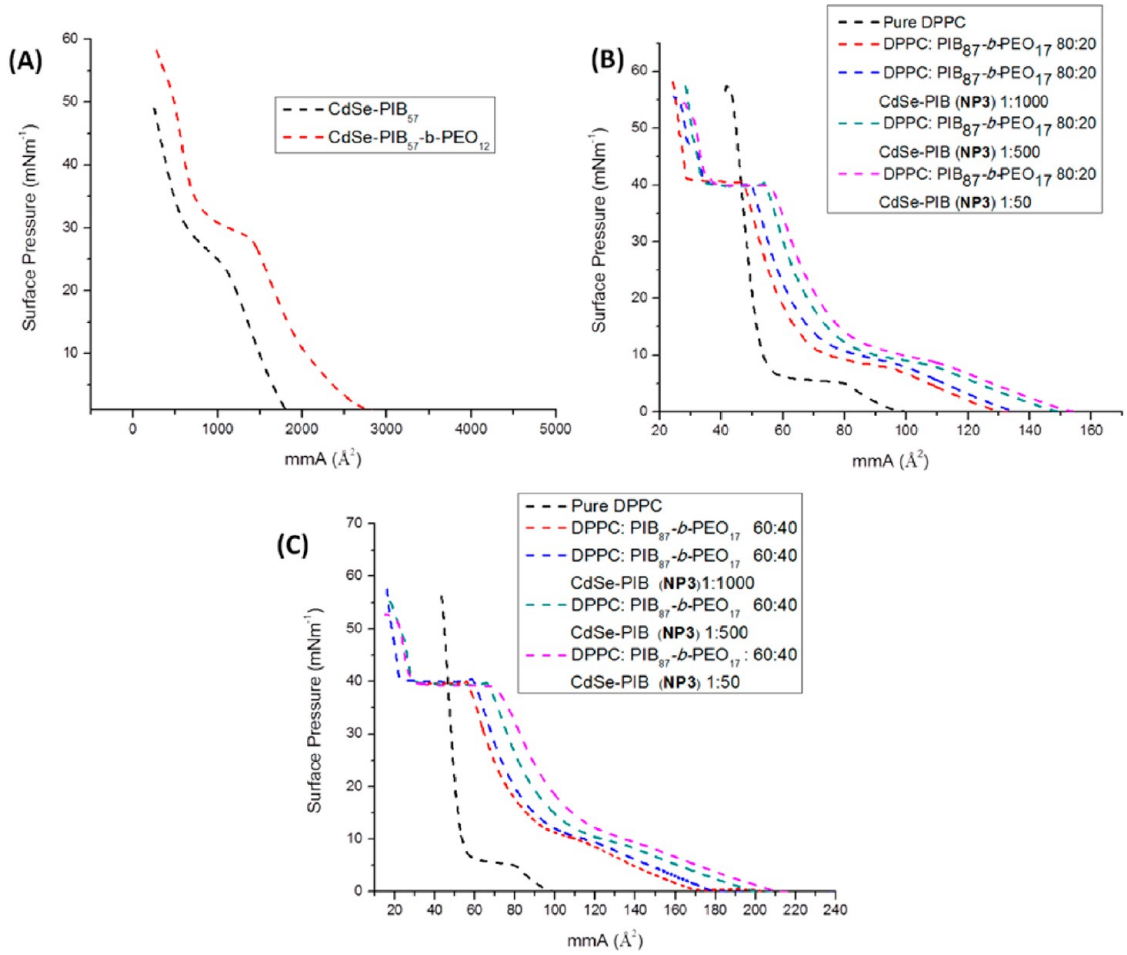

Figure 2. Langmuir monolayer isotherms of pure NPs and DPPC:PIB_{87}-*b*-PEO_{17} mixtures with NPs. (A) Hydrophobic PIB_{57}-covered CdSe NPs (NP3) (black curve) and PIB_{57}-*b*-PEO_{12}-covered CdSe NPs (NP5) (red curve). (B) Mixture of DPPC:PIB_{87}-*b*-PEO_{17} in the ratio 80:20 mol % with hydrophobic PIB-covered CdSe NPs (NP3) at different ratios. (C) Mixture of DPPC:PIB_{87}-*b*-PEO_{17} in the ratio 60:40 mol % with hydrophobic PIB-covered CdSe NPs (NP3) at different ratios.

In comparison to the isotherms of the pure DPPC and PIB_{87}-*b*-PEO_{17} BCP, which have been reported in the literature,[38,52] the first significant increase in surface pressure of the hydrophobic PIB-covered CdSe NPs (**NP3**) was observed at a mean molecular area (mmA) of 1900 Å^2 (see Figure 2A, black curve). In an attempt to generate the full nanoparticle isotherm, increased amounts of NP were deposited at the air/water interface. Regardless of the amount of material deposited, we did not observe any monolayer collapse in which particle movement out of the monolayer was apparent. In all cases the barrier moved into the minimum area position without the monolayer showing any collapse point. This demonstrates that the particles are unable to form a two-dimensional rigid phase, which would break upon sufficient compression. Such behavior might be a result of a NP multilayer stack formation, which could be clearly seen by comparing the AFM height image of a transferred NP monolayer at 30 mN m^{-1} with that at 20 mN m^{-1} (see Supporting Information Figure S6).

The interaction of hydrophobic PIB-covered CdSe NPs (**NP3**) with mixed DPPC:PIB_{87}-*b*-PEO_{17} (80:20 or 60:40 mol %) membranes was first investigated using a

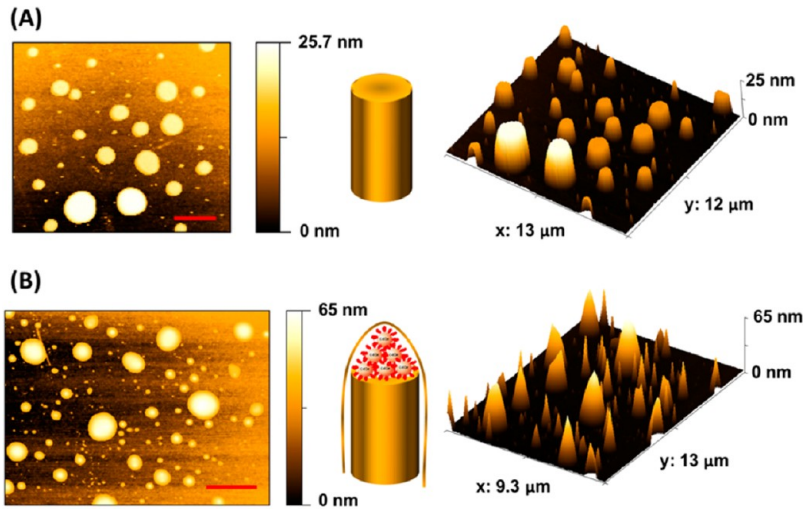

Figure 3. AFM height image of a mixed DPPC:PIB_{87}-*b*-PEO_{17} monolayer in the ratio 80:20 mol % transferred at a surface pressure of 30 mN m^{-1} (A) without NPs and (B) with hydrophobic PIB-covered CdSe NPs (NP3). Scale bar represents 2.5 μm.

monolayer that mimics half a bilayer membrane. The effect of an increased nanoparticle loading on mixed DPPC:PIB_{87}-*b*-PEO_{17} monolayers was investigated, as shown in Figure 2B and C. In the 80:20 mol % mixture without nanoparticles (red curve), it can be seen that the amphiphilic PIB_{87}-*b*-PEO_{17} copolymer molecule impacts the rearrangement behavior of the lipid molecules at the air/water interface, which results in the disturbance of the lipid packing, leading to a shift of the LE/LC transition plateau of DPPC to higher surface pressures (compare DPPC isotherm, black curve). A flattening of the isotherm of the 80:20 mol % mixture was observed in the low-pressure region between 0 and 8 mN m^{-1}, as the BCP chains support the persistence of the expanded phase of the lipid monolayer.

In the 80:20 mol % mixture with increasing amount of nanoparticles, 1:1000 (blue), 1:500 (green), and 1:50 (purple), with respect to PIB_{87}-*b*-PEO_{17}, the nanoparticles shift the isotherm of the 80:20 mixture to higher areas per molecule. This indicates that the incorporation of the polyisobutylene-covered CdSe NPs (**NP3**) into the 80:20 mol % mixed monolayer reduces the free area of the DPPC and PIB_{87}-*b*-PEO_{17}, showing a lift-off at higher areas per molecule. As a result of the NP penetration into the mixed monolayer, the lift-off in the isotherm related to the compression of the liquid-expanded (LE) phase occurs at a higher area per molecule as the amount of nanoparticles increases. Considering the LE/liquid-condensed (LC) coexistence phase, incorporation of the PIB-covered CdSe NPs makes the LE/LC coexistence phase less flattened with increasing NP amounts. This might be interpreted as a result of hindering of the phase transition. A similar behavior was observed for the hydrophobic nanoparticles (**NP3**) interacting with mixed 60:40 mol % monolayer (see Figure 2C).

In order to locate the position of the hydrophobic NPs (**NP3**) in phase-separated DPPC:PIB_{87}-*b*-PEO_{17} monolayers,[38] where we know that the copolymer domains are getting larger with increasing copolymer content, AFM investigations were performed using the Langmuir–Blodgett (LB) technique. Thus, monolayers of DPPC:PIB_{87}-*b*-PEO_{17} 80:20 or 60:40 mol % with hydrophobic PIB-covered CdSe NPs (**NP3**) (NP/PIB_{87}-*b*-PEO_{17} = 1:1000) were transferred onto silicon substrates at 30 mN m^{-1} (comparable to the internal pressure of biological membranes).[53] Interestingly, the 80:20 mol % mixture without nanoparticles shows cylindrical-shaped mesomorphic PIB domains surrounded by the lipid monolayer, mostly dominated with a height of ~11 nm, which scales exactly with a single-folded PIB chain, and other columns with a ~22 nm height, corresponding to a fully stretched PIB chain, as explained in the litrature[54] (see Figure 3A). The incorporation of **NP3** induces a morphological change of the cylindrical-shaped PIB columns into a cone-like structure with increased total heights up to ~65 nm. These findings match with a hierarchical assembly in which the NPs are found to be selectively located on top of the PIB columns, forming three to eight NP stacks, as illustrated in Figure 3B. In contrast, the observed cone-like polymer domains in a 60:40 mixture (Figure 4) (DPPC:PIB_{87}-*b*-PEO_{17}) have heights up to ~130 nm. A change in height of about 100 nm observed in the 60:40 mol % DPPC:PIB_{87}-*b*-PEO_{17} mixtures can be explained by the higher absolute amount of polymer in comparison to the 80:20 mixture. As the domain sizes and the number of domains are the same in both mixtures (80:20 and 60:40) and the fraction of the NPs/polymer stays constant (1:1000), the formation of higher NP stacks in comparison to the 80:20 mixture (DPPC:PIB_{87}-*b*-PEO_{17}) results. Additional interfacial effects could be responsible for the same number of domains in both cases.

Interaction and Location of Amphiphilic CdSe NPs (NP5) in Hybrid Monolayers. When compared to the isotherm of

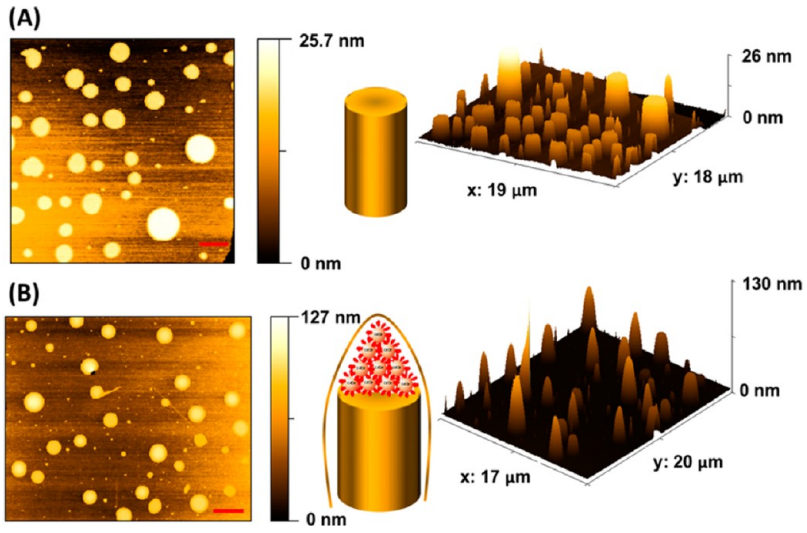

Figure 4. (A) AFM height image of a mixed DPPC:PIB$_{87}$-*b*-PEO$_{17}$ monolayer in the ratio 60:40 mol % transferred at a surface pressure of 30 mN m^{-1} (A) without NPs and (B) with hydrophobic PIB-covered CdSe NPs (NP3). Scale bar represents 2.5 μm.

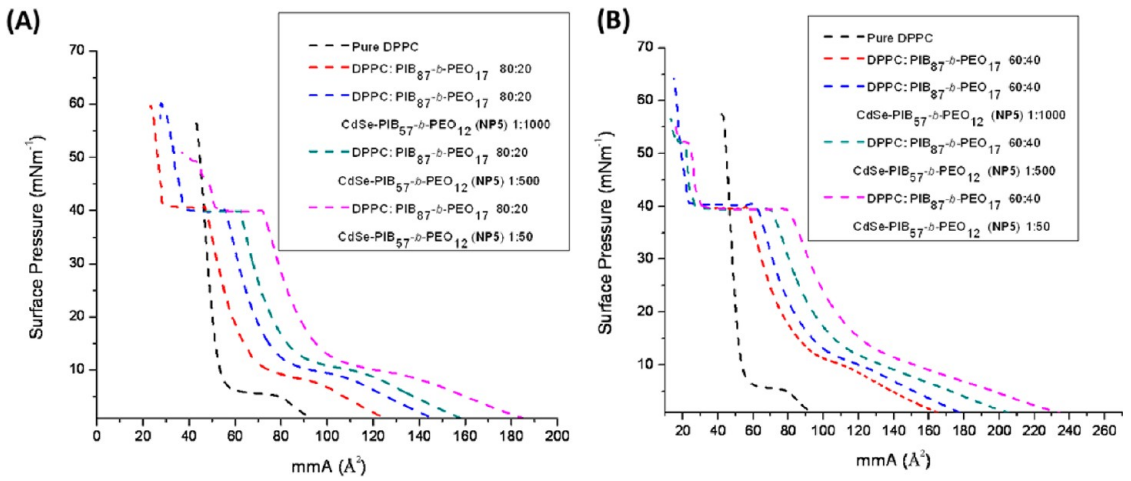

Figure 5. Langmuir monolayer isotherms of DPPC:PIB$_{87}$-*b*-PEO$_{17}$ mixtures with NPs. (A) mixture of DPPC:PIB$_{87}$-*b*-PEO$_{17}$ in the ratio 80:20 mol % with amphiphilic PIB$_{57}$-*b*-PEO$_{12}$-covered CdSe NPs (NP5) at different ratios. (B) Mixture of DPPC and PIB$_{87}$-*b*-PEO$_{17}$ in the ratio 60:40 with amphiphilic PIB$_{57}$-*b*-PEO$_{12}$-covered CdSe NPs (NP5) at different ratios.

PIB-covered CdSe NPs (**NP3**), the isotherms of the amphiphilic PIB$_{57}$-*b*-PEO$_{12}$-covered CdSe NPs (**NP5**) showed a first significant rise in surface pressure at mmA of 2800 Å^2, which might be considered as a gas-to-liquid transition or sponge phase, followed by a continuous increase in the surface pressure and a pseudoplateau at 30 mN m^{-1} (Figure 2A (red)). The isotherm also did not show any collapse as the barrier moved into the minimum area position without the monolayer showing any collapse point.

Incorporation of amphiphilic nanoparticles (**NP5**) into mixed DPPC:PIB$_{87}$-*b*-PEO$_{17}$ (80:20 or 60:40 mol %) membranes resulted in a significant disturbance of the lipid packing, shifting the isotherms of both the 80:20 and the 60:40 mol % mixtures to higher areas per molecule with increasing **NP5** ratio. This favors an earlier molecule packing at higher mmA values. The LE/LC coexistence region was less pronounced and shifted to higher surface pressure with increased **NP5** ratio as observed before in the case of **NP3** (see Figure 5A and B). This can be explained by the fact that the PEO block length (12 units) of the amphiphilic **NP5** is able to anchor the NPs to the air/water interface, but is not long enough to induce further effects on the phase transition state of the mixed monolayer, thus leading to a similar isothermal behavior when using **NP3**.

A monolayer of the ternary mixture of 80:20 mol % DPPC:PIB$_{87}$-*b*-PEO$_{17}$ and amphiphilic NPs (**NP5**) was transferred onto silicon substrates and scanned with AFM. The AFM result (Figure 6B) revealed that amphiphilic NPs (**NP5**) induce a morphological change of the cylindrical-shaped PIB columns into cone-like structures with height increases from ~24 nm up to 51 nm, similar to that observed for **NP3**. It should be noticed that the amphiphilic covered CdSe NPs could be located in the polymer-rich areas as well as in the lipid-rich areas of

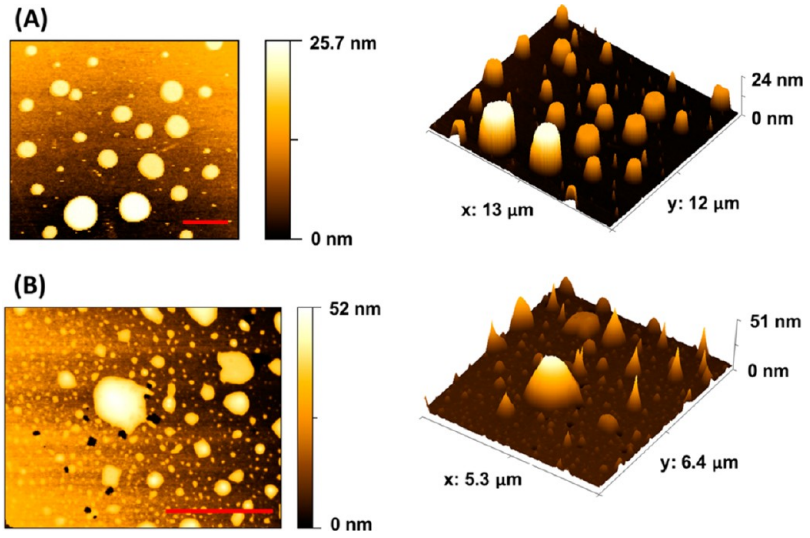

Figure 6. AFM height image of mixed DPPC:PIB_{87}-*b*-PEO_{17} monolayers in the ratio 80:20 mol % transferred at a surface pressure of 30 mN m^{-1} (A) without NPs and (B) with amphiphilic PIB_{57}-*b*-PEO_{12}-covered CdSe NPs (NP5) transferred at a surface pressure of 30 mN m^{-1}. Scale bar represents 2.5 μm.

the monolayer. The small cone-like domains, as seen in the 3D height image of Figure 6B, are nearly homogeneously distributed in the transferred monolayer, which might be nanoscopic stacks of amphiphilic NPs being anchored to the silicon substrate by their short PEO chains.

Fluorescence Microscopy of Hydrophobic Rhodamine-B-Labeled CdSe NPs (NP6) within Hybrid Monolayers. To prove the AFM results of transferred hybrid monolayers (composed of lipid, polymer and functionalized NPs), the morphology of these ternary mixed monolayers at the air/water interface was monitored by fluorescence microscopy using fluorescent-labeled hydrophobic CdSe NPs, similar to the morphology studies of binary mixed monolayers consisting of DPPC and PIB_{87}-*b*-PEO_{17} BCP, which was reported previously.[38] It was shown that mixed monolayers from 10 to 40 mol % of the diblock copolymer component demonstrate phase separation phenomena over the whole compression range.

Initially, at low surface pressures ($\pi \leq 4$ mN m^{-1}) polymer-rich domains appeared completely round surrounded by the LE phase of DPPC showing a uniform fluorescence intensity signal of the rhodamine-B labeled lipid. Further compression of the film passing the well-known plateau region of DPPC (LE/LC transition)[52] forms pure LC domains of the lipid molecules. An increase in the polymer content of mixed monolayers showed that the DPPC transition plateau was shifted to higher surface pressures, attributed to the BCP molecules, which support the persistence of the liquid-expanded phase of the lipid monolayer. Typically with increasing polymer content, we also observed that the separation process between the lipid and polymer molecules led to an increase in size of the polymer-rich domains.[38] In the present study, the goal of our work was to investigate the location of functionalized NPs in phase-separated lipid/polymer films depending on the monolayer compression state. We therefore have labeled hydrophobic NPs (**NP3**) with rhodamine-B, thus generating **NP6**, which allowed the simultaneous monitoring of the localization of the labeled NPs in the phase-separated film. Fluorescence monolayer microcopy of lipid/polymer mixtures (80:20 mol %) treated with fluorescent-labeled hydrophobic NPs (**NP6**) (NP to polymer ratio of 1 to 1000) revealed essentially the same hierarchical morphologies as observed by transferred monolayers (AFM studies). Figure 7 presents fluorescence microcopy images of ternary mixed monolayers recorded at different surface pressures.

At low surface pressures (below 6 mN m^{-1}), we found only slight differences in the grayscale level of the monolayer images, corresponding to the formation of round polymer-rich domains (dark gray spots) in the liquid-expanded DPPC film (light gray). The observed small differences in brightness indicate that the NPs are nearly homogenously distributed in the lipid/polymer monolayer, showing no preferential location at low compression states of the films. With further compression of the monolayer passing the LC/LE phase transition of DPPC the nucleation and growth of pure DPPC LC domains occurred (see Figure 7C–E). These completely black-colored domains indicate a change of the NP miscibility with the lipid-rich areas so that the NPs are excluded from the LC monolayer regions. At higher surface pressures (above 12 mN m^{-1}) the NPs start to move on top of the polymer-rich domains, as clearly visible in Figure 7F, by displaying a very bright edge of the polymer domains. Obviously, the attractive interaction between the PIB columns formed by the PIB_{87}-*b*-PEO_{17} and the PIB corona of the NPs leads to such hierarchical ordering at the

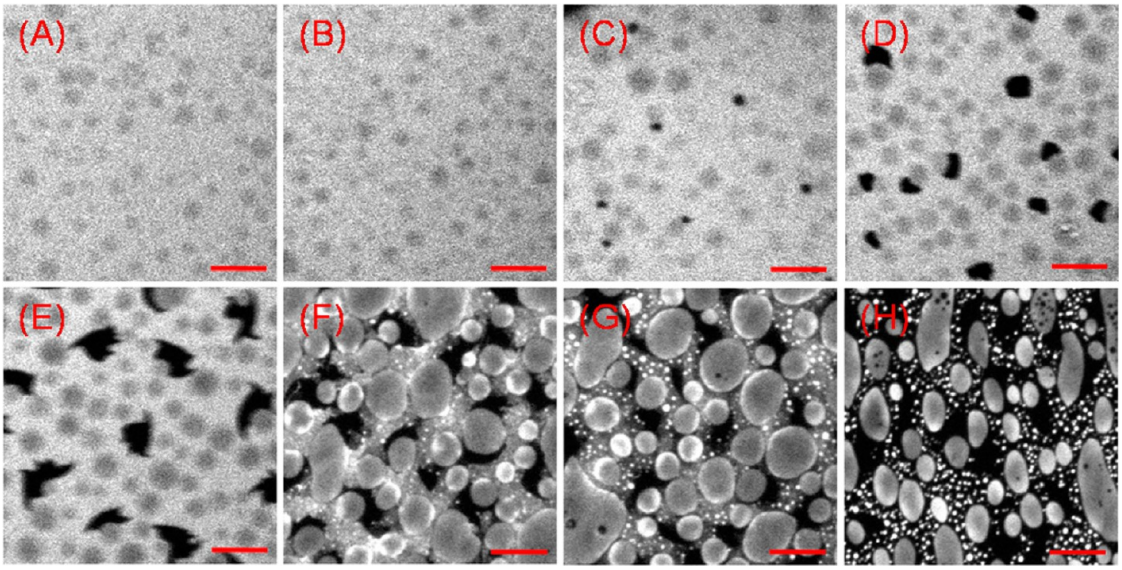

Figure 7. Fluorescence microscopy images of mixed DPPC:PIB_{87}-*b*-PEO_{17} monolayers 80:20 mol % at the air/water interface (20 °C) mixed with fluorescent-labeled NPs (NP6) to monitor their location and behavior depending on the compression state of the film. The images were recorded at surface pressures of 2.7 mN m^{-1} (A), 6.1 mN m^{-1} (B), 8.2 mN m^{-1} (C), 8.7 mN m^{-1} (D), 9.4 mN m^{-1} (E), 11.5 mN m^{-1} (F), 12.4 mN m^{-1} (G), and 30.1 mN m^{-1} (H). Scale bars represent 16 μm.

air/water interface. Fluorescence microscopy images at higher compression states of the ternary mixed monolayers (~30 mN m^{-1}) demonstrated that the NPs (**NP6**) are selectively located on top of the polymer-rich domains, showing a nearly homogeneous fluorescence intensity signal (polymer domains perceptibly increased in brightness; Figure 5H). The initial homogeneous distribution of hydrophobic NPs in lipid/polymer monolayers varies strongly with increasing surface pressure. As mentioned earlier, the formation of pure DPPC (LC phase) domains already in the low surface pressure region (~12 mN m^{-1}) leads to the selective location of the hydrophobic NPs in the polymer-rich areas of the phase-separated film, which demonstrates their attractive interaction. The final increase in brightness of the polymer domains at high surface pressures (30 mN m^{-1} and above), indicated by a nearly homogenously bright color of the polymer domains, confirms the result of our AFM studies revealing the hierarchical ordering of the NPs on top of the BCP chains at the air/water interface.

Monolayer Adsorption Experiments of Hydrophilic CdSe NPs (NP4) on Pure and Mixed DPPC:PIB_{87}-*b*-PEO_{17} Monolayers. Since the interaction of hydrophilic PEO-covered NPs (**NP4**) with the mixed DPPC:PIB_{87}-*b*-PEO_{17} BCP monolayer could not be investigated *via* Langmuir film balance measurements due to their excellent water solubility preventing any determination of a stable Langmuir isotherm, we have decided to investigate the effect of water-soluble CdSe NPs on pure DPPC, pure PIB_{87}-*b*-PEO_{17} BCP, and mixed DPPC/PIB_{87}-*b*-PEO_{17} monolayers by conducting monolayer adsorption measurements. Changes in the surface pressure as a function of time after injecting hydrophilic PEO-covered CdSe NPs (**NP4**) into the subphase below the spread monolayers of pure DPPC (black curve) (see Figure 8), pure PIB_{87}-*b*-PEO_{17} BCP (red curve), or binary mixtures (DPPC:PIB_{87}-*b*-PEO_{17} with 20 mol % (blue curve) or 40 mol % BCP (green curve)) caused by the surface adsorption of **NP4** are shown in Figure 6. The starting surface pressure (π_0) values were determined at time zero, which corresponds to the injection time of the NPs into the subphase. From the adsorption measurement, it is obvious that immediately after injection of the PEO-covered CdSe NPs (**NP4**) the surface pressure starts to increase until an equilibrium value (π_{eq}) is reached, where a significant increase in the surface pressure could no longer be observed. The change in the surface pressure ($\Delta\pi$ ($\Delta\pi = \pi_{eq} - \pi_0$)) of all samples indicates that the PEO-covered NPs (**NP4**) were rapidly adsorbed onto the hydrophilic portion of the monolayer at the air/water interface (*i.e.*, displaying surface activity), where they can interact with the DPPC head groups and compete for area to occupy.

Changes in surface pressure, $\Delta\pi$, that were observed for pure PIB_{87}-*b*-PEO_{17} BCP monolayers were not as large as compared to pure DPPC films at the same starting surface pressure, π_0. This could be explained by the fact that the PEO chains of the BCPs are dissolved and stretched into the subphase, which forms a barrier, thus preventing the hydrophilic NPs from coming up to the interface, which has an effect on the rearrangement behavior of the BCP chains (see schematic illustrations in Figure 8).

Interestingly, the binary mixture of DPPC and the PIB_{87}-*b*-PEO_{17} BCP using either 20 or 40 mol % of the polymer component showed that with increasing polymer content the changes in the surface pressure ($\Delta\pi$)

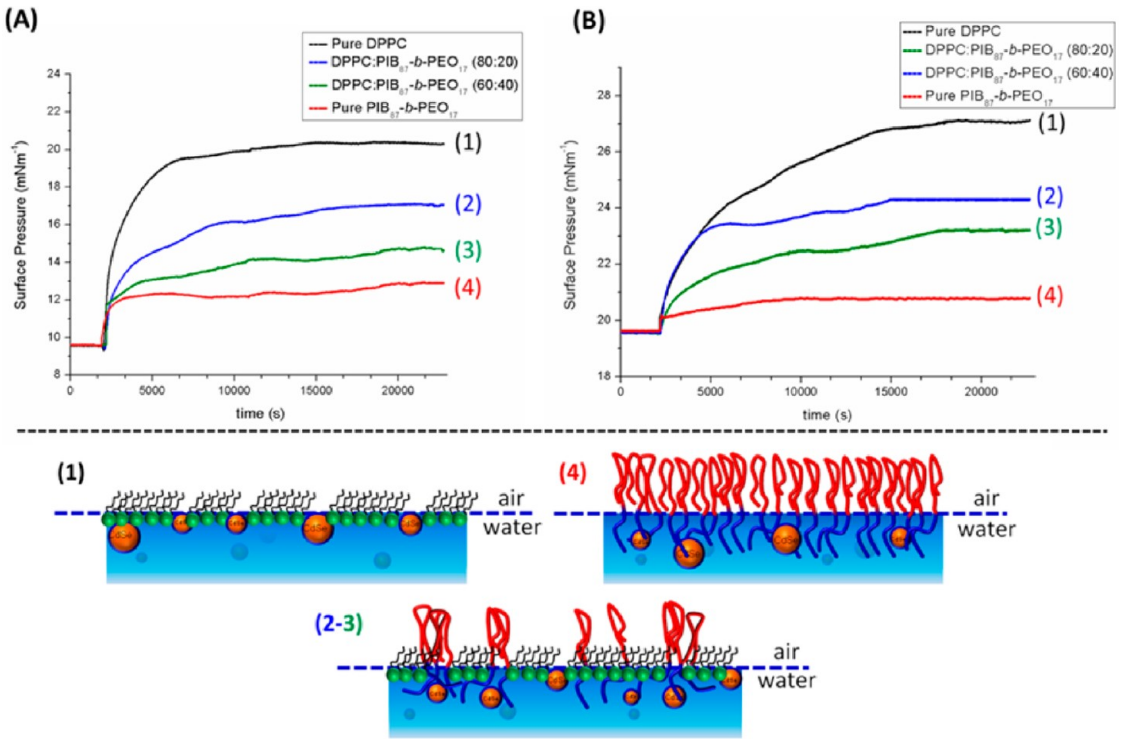

Figure 8. Time-dependent Langmuir adsorption isotherms of NP4 injected into the subphase at 20 °C of monolayers of pure DPPC (black curve), pure PIB_{87}-*b*-PEO_{17} (red curve), and mixtures of DPPC:PIB_{87}-*b*-PEO_{17} at 20 mol % (blue) and 40 mol % (green) PIB_{87}-*b*-PEO_{17} BCP at initial surface pressures of (A) approximately 10 mN m^{-1} and (B) 20 mN m^{-1}.

decrease drastically, which implies less interaction of the NPs with the molecules at the interface. This is in good agreement with the observations as obtained for pure polymer films, which showed minimal influence on the molecule organization by surface-adsorbed **NP4**, demonstrating attractive interactions between the PEO chains of the BCP and the functionalized NP shell, which keep the water-soluble NPs away from the air/water interface. The high affinity of the PEO-functionalized NPs (**NP4**) towards the hydrophilic portion of the BCP molecules is clearly seen by comparing the changes in surface pressure with increasing polymer content (see Supporting Information Table S1), assuming that the PEO chains of the BCP in phase-separated lipid/polymer monolayers submerged into the subphase might serve as an attractive barrier for the PEO-covered NPs (**NP4**), preventing interactions with DPPC domains. The starting pressure at which the NPs were injected (compare Figure 8, measurements at 10 and 20 mN m^{-1}) influences the magnitude of surface pressure changes ($\Delta\pi$) when nanoparticles were injected, demonstrating that the molecule packing density at the air/water interface regulates the penetration ability of the hydrophilic CdSe NPs.

Bilayer Investigations: Incorporation of Hydrophobic NPs into Hybrid Bilayer Membranes. As the monolayer studies of hydrophobic (PIB), hydrophilic (PEO), and amphiphilic (PIB-PEO) functionalized CdSe NPs with mixed lipid/polymer membranes composed of DPPC and the PIB_{87}-*b*-PEO_{17} block copolymer have shown selective interactions depending on the NP surface hydrophobicity, the controlled localization of hydrophobic PIB-modified CdSe NPs within the polymer domains was extended into a bilayer system using giant unilamellar vesicles (GUVs) consisting of DPPC and the PIB_{87}-*b*-PEO_{17} BCP. Such a designed amphiphilic block copolymer, when incorporated into gel-phase vesicles of DPPC, has been shown to induce different membrane morphologies by varying the lipid to polymer composition.[38] The membrane morphology of these hybrid vesicles appears uniform when prepared from mixtures below 20 mol % and above 30 mol % of the BCP component. In contrast, we have observed a phase-separated membrane morphology in the narrow compositional range between 20 and 28 mol % of BCP, resulting in the formation of lipid- and polymer-rich domains. Since NPs with diameters smaller than 8 nm are not expected to induce disruption of DPPC bilayer membranes,[6,13] we investigated the incorporation of hydrophobic CdSe NPs into our well-investigated hybrid membrane system, addressing the specific NP location with respect to the lipid/polymer mixing ratio and the resulting membrane morphology. Additionally, the size (~ 6 nm) of the NPs was expected further to drive a selective localization of the NPs into the BCP phase.

Hybrid GUVs with incorporated **NP6** were formed by a modified electroformation method as originally reported by Angelova *et al.*[55] using a NP to lipid ratio of 1 to 1500. Since we expected that the incorporation of

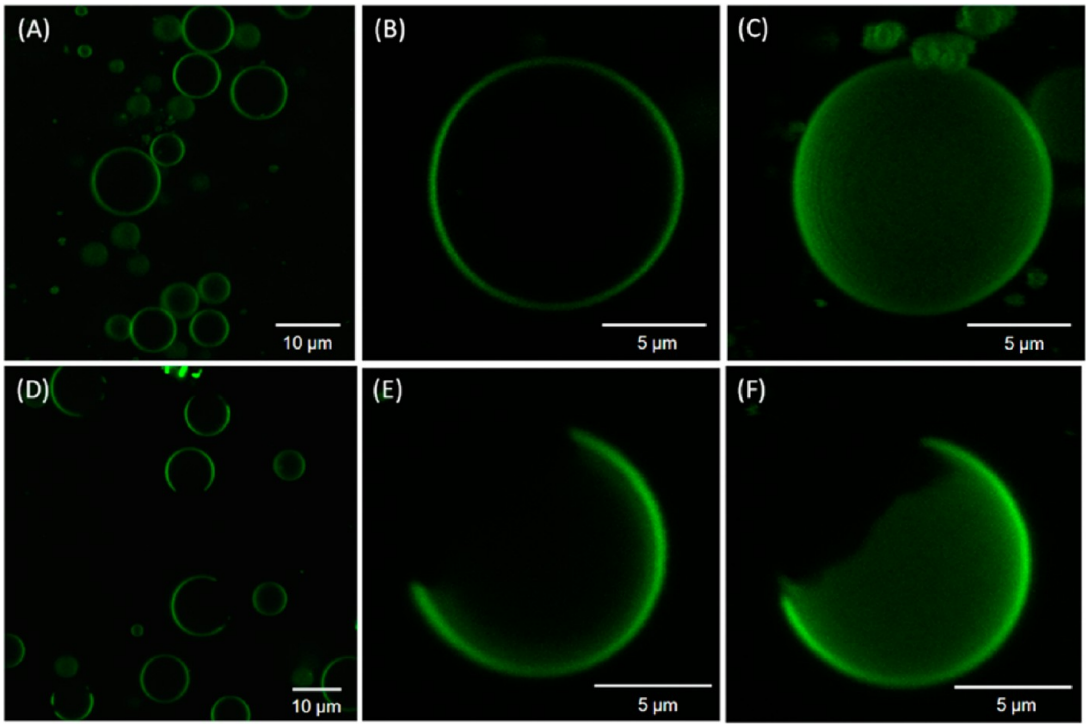

Figure 9. Confocal microscopy images of mixed (A−C) and phase-separated hybrid GUVs (D−F) composed of DPPC and the PIB_{87}-*b*-PEO_{17} BCP with incorporated hydrophobic CdSe NPs (NP6) (NP to lipid ratio of 1 to 1500), demonstrating differences in the phase labeling behavior of the monitored fluorescent-labeled NPs by varying the lipid to BCP composition. Panels (A), (B), and (C) show an overview and single GUV images of mixed hybrid GUVs at RT, which were obtained from a 84:16 mol % mixture of DPPC with BCP, proving that the incorporated fluorescent CdSe NPs (NP6) (green, excited at 561 nm) are localized in the whole vesicle membrane. In panel (C), the 3D reconstruction of an axial series of confocal slices from the single GUV in (B) clearly demonstrates the uniform fluorescent intensity signal of the labeled NPs (green) in the hybrid GUV membrane. Panels (D), (E), and (F) depict an overview and single GUV images of phase-separated hybrid GUVs at RT obtained from a 80:20 mol % mixture of DPPC with BCP, monitoring the fluorescent-labeled NPs. The fluorescent CdSe NPs preferentially partition into one of the two prevailing phases (black and green patches), as clearly shown in the 3D recontruction of a single GUV in panel (F).

hydrophobic NPs will basically depend on the prevailing membrane morphology, a selective incorporation of the PIB-modified NPs into the polymer-rich phases should be observed. Therefore, we have chosen two different lipid/polymer mixing ratios, one showing a mixed (16 mol % BCP) and the other a phase-separated membrane morphology (20 mol % BCP), as shown in Figure 9.

For the 84:16 mol % mixture of lipid with BCP, the obtained hybrid GUVs with incorporated hydrophobic NPs (NP to lipid ratio = 1 to 1500) clearly demonstrate a uniform membrane morphology, which is visualized by monitoring the excited **NP6** (excited at a wavelength of 561 nm). The obtained hybrid GUVs remain stable, and no disruption of the bilayer membrane was observed for this NP to lipid ratio. As depicted in Figure 9B and C, the PIB-modified CdSe NPs are uniformly embedded within the whole hybrid bilayer, showing a single-phase membrane.

In contrast, we observed for the 80:20 mol % mixture of DPPC with PIB_{87}-*b*-PEO_{17} upon cooling to room temperature the formation of phase-separated membrane morphologies (Figure 9D−F). Monitoring the fluorescent-labeled NPs (**NP6**), which are preferentially incorporated into one of the two prevailing phases (green-colored domains; see overview image in Figure 9 D) we can attribute these domains to the polymer-rich phases. This is most likely, considering the fact that the polymer-functionalized NPs (**6**) exhibit a brush of polyisobutylene chains on their surface and should therefore be selectively incorporated into the polymer-rich domains.

Consequently, we drew the conclusion that the dark domain in the hybrid GUV membrane, as shown in Figure 9F, is the lipid-rich phase showing no fluorescence signal of the **NP6**. These domains appear upon cooling to room temperature below the transition temperature of DPPC (T_m = 41.6 °C), indicating that at room temperature (RT) the demixing process leads to the formation of more ordered lipid-rich domains,[56] which are depleted of polymer molecules. In contrast, at high temperatures (above T_m of DPPC) the hybrid bilayer is in a fluid state showing complete mixing.

CONCLUSION

We have thoroughly investigated the interaction of surface-grafted nanoparticles (CdSe, size 2 nm) with mixed monolayers, thus probing the different states of interaction between nanoparticles and mixed lipid/polymer membranes. As surface hydrophobicity plays

a significant role in controlling the interaction between nanoparticles and lipid membranes, we demonstrate the preparation and characterization of polymer-functionalized CdSe NPs, based on ligand exchange of pyridine-covered CdSe nanoparticles with end group-functionalized polymers, bearing phosphine oxide ligands for polymer chain attachment. As proven by DLS, TGA, NMR, and IR experiments, grafting of either hydrophobic (PIB), hydrophilic (PEO), or amphiphilic (PEO-PIB) chains onto the nanoparticles with grafting densities of ~0.5 chains/nm^2 can be achieved. Thus, the selective interaction of nanoparticles with mixed lipid/polymer membranes from 1,2-dipalmitoyl-*sn*-glycero-3-phosphocholine and PIB_{87}-*b*-PEO_{17} block copolymer was demonstrated, depending purely on the type of NP surface. It was observed that hydrophobic PIB-modified CdSe NPs can be selectively located within polymer domains in a mixed lipid/polymer monolayer at the air/water interface by changing their typical domain morphology, while amphiphilic PIB-PEO-modified CdSe NPs showed no specific localization in phase-separated lipid/polymer films. As a result, AFM experiments of transferred monolayers could clearly demonstrate the specific "piling up" of the nanoparticles **NP3** on top of the separated PIB columns formed upon compression of the mixed monolayer. In addition, hydrophilic water-soluble PEO-modified CdSe NPs can readily adsorb onto spread monolayers, showing a larger effect on the molecular packing at the air/water interface in the case of pure lipid films compared to mixed monolayers. On the basis of attractive interactions between the polymer shell of the NPs and the hydrophilic block copolymer chains, the NPs were shielded from lipid domains being merged with the BCP PEO chains in the subphase. Bilayer investigations using hybrid GUVs demonstrate that PIB-modified CdSe NPs were selectively incorporated into polymer-rich phases when incorporated into a DPPC:PIB_{87}-*b*-PEO_{17} mixture, which by itself initially formed phase-separated membrane morphologies. Preferential incorporation is a result of the formation of PIB brushes on the polymer-functionalized NP surfaces (**NP6**), which leads to the specific location within the PIB phase of the BCP. Consequently, we could prove that the selective interactions between functionalized NPs and polymer domains in mixed lipid/polymer mono- and bilayers are possible by simply tuning the appropriate interfacial energies between the NP surfaces and the interacting membrane components. Thus, understanding the incorporation of nanoparticles into specific parts of bilayer membranes. The achieved results open a new prospect for subtle engineering of membranes, their nanoporosity, (nano-) domain structure, and mechanical properties serving as a model system in designing functional nanomaterials for effective nanomedicine or drug delivery.

EXPERIMENTAL SECTION

Materials. *Solvent and Reagents.* All chemicals were purchased from Sigma-Aldrich (Schnelldorf, Germany) and were used as received unless otherwise stated. All solvents, which were used for the synthesis of the diblock copolymer and workup procedures, were distilled prior to use. Toluene and tetrahydrofuran (THF) were predried over potassium hydroxide for several days, refluxed over sodium/benzophenone, and freshly distilled under an argon atmosphere. The PIB-PEO diblock copolymer (PIB_{87}-*b*-PEO_{17}; $M_{n(NMR)}$ = 5900 g/mol determined by ^{1}H NMR) with a minimal polydispersity (PDI ≤ 1.2), used in this study, was synthesized in our laboratories *via* a combination of a living carbocationic polymerization method and the approach of the azide/alkyne "click" reaction, as reported previously.[38] 1,2-Dipalmitoyl-*sn*-glycero-3-phosphocholine (M_n = 734.05 g/mol) was purchased from Avanti Polar Lipids (Alabaster, AL, USA) and used without further purifications.

Measurements. *Langmuir Film Technique.* Surface pressure (π) measurements of the pure compounds and of different binary mixed systems of PIB-PEO BCP, DPPC, and NPs at the air/water interface were performed using a Langmuir trough system (KSV, Helsinki, Finland) with a maximum available surface of 76.800 mm^2. To minimize dust, the trough was kept in a closed box. The used subphase (water) was purified by a Purelab Option system (ELGA Ltd., Celle, Germany). Before each measurement was started the trough was purified four times with distilled water and two times with ultrapure water (total organic carbon <5 ppm; conductivity <0.055 μS/cm). All compression measurements were performed at a constant temperature (20 °C) achieved by a circulating water bath system. The investigated mixture of copolymers, DPPC, and NPs was dissolved in chloroform (HPLC grade, Sigma Aldrich, Schnelldorf Germany) at a concentration of 1 mM. Defined amounts of the prepared solutions (different molar ratios of DPPC to BCP and NPs) were spread on the subphase using a digital microsyringe (Hamilton, Schnelldorf Germany). Afterward, each surface pressure measurement using a compression rate of 5 mm/min was started 15 min after spreading to ensure full evaporation of the solvent and a uniform monolayer formation.

Fluorescence Microscopy Monolayer Investigations. Fluorescence microscopy imaging of monolayers at the air/water interface was performed using an "Axio Scope.A1 Vario" epifluorescence microscope (Carl Zeiss MicroImaging, *Jena*, Germany). The microscope was equipped with a Langmuir Teflon trough with a maximum area of 264 cm^2 and two symmetrically moveable computer-controlled Teflon barriers (Riegler & Kirstein, Berlin, Germany). The trough was positioned on an *x-y* stage (Märzhäuser, Wetzlar, Germany) to be able to move the film balance with respect to the objective lens to any desired surface position. The *x-y-z* motion control was managed by a MAC5000 system (Ludl Electronic Products, Hawthorne, NY, USA). The trough was enclosed with a home-built Plexiglas hood to ensure a dust-free environment, the temperature of 20 °C was maintained with a circulating water bath, and the whole setup was placed on a vibration-damped optical table (Newport, Darmstadt, Germany). The air/water surface was illuminated using a 100 W mercury arc lamp with a long-distance objective (LD EC Epiplan-NEOFLUAR 50×), and the respective wavelengths were selected with a filter/beam splitter combination, which is appropriate for the excitation and detection of Rh-DHPE (Zeiss filter set 20: excitation band-pass BP 546/12 nm, beam splitter FT 560 nm, emission band-pass BP 575−640 nm). Images were recorded using an EMCCD camera (Image EM C9100-13, Hamamatsu, Herrsching, Germany). Image analysis and data acquisition was done using AxioVision software (Carl Zeiss MicroImaging, Jena, Germany). All presented images show areas of individually contrast-adjusted raw data. Monolayer

films of DPPC/BCP/NPs mixtures and pure compounds were prepared with an entire spreading concentration of 1 mM in chloroform (HPLC-grade, Carl Roth, Karlsruhe, Germany). The concentration of the fluorescent-labeled rhodamine−DHPE in the spreading solution was 0.01 mol % and was used for all measurements. Microscopy images were taken during compression of the monolayer using a compression speed of 4.6 cm^2/min.

UV−Vis Measurements. UV−vis spectra were recorded using a PerkinElmer Lambda 18 UV−vis spectrometer. The samples were dissolved in $CHCl_3$ (HPLC-grade purchased from VWR Darmstadt Germany) in a concentration of 0.5 mg/mL.

Adsorption Measurements. Adsorption experiments at the air/water interface were carried out at 20 °C at different initial surface pressures of pure DPPC, pure PIB_{87}-*b*-PEO_{17} block copolymer, and a mixture of DPPC: PIB_{87}-*b*-PEO_{17} block copolymer (with diblock copolymer amounts of 20 and 40 mol %) monolayers on a circular Langmuir trough with a diameter of 3 cm, a depth of 1.39 cm, and a subphase volume of 10.25 mL (Riegler & Kirstein, Berlin, Germany). For preparation of the pure and mixed monolayers, a defined amount in HPLC-grade $CHCl_3$ was spread with a digital Hamilton microsyringe onto the water subphase of Millipore quality (total organic carbon <5 ppm; conductivity <0.055 μS/cm). After waiting for 20 min for complete solvent evaporation and uniform dispersion of the monolayer molecules at the air/water interface, 10 μL of the water-soluble hydrophilic CdSe nanoparticles (25 or 5 mg/mL) was injected into the subphase below the monolayers through a channel located at the bottom of the Langmuir trough. In order to ensure a homogeneous bulk concentration of NPs in the subphase and in order to avoid large perturbations at the air/water interface, the subphase was gently stirred with a small rolling sphere. The changes of surface pressure (mN/m) at the air/water interface caused by the injected aqueous solution of NP were monitored as a function of time (seconds) by measuring initial and final surface pressure using a filter paper as a Wilhelmy plate.

Atomic Force Microscopy. Surface topography of LB films was studied using an atomic force microscope working in tapping mode with silicon cantilevers. Cantilevers were of type TESPA (NanoWorld, Switzerland) and had a nominal resonance frequency of about 285 kHz and an average spring constant of about 42 N/m.

Dynamic Light Scattering. DLS measurements were performed in chloroform solutions of the NPs after dilution by ~1/50 with pure solvent on a Viscotek 802 using OmniSIZE software.

FTIR Measurement. Infrared measurements were performed on a Bruker Vertex 70 FT-IR spectrometer (Bruker, Leipzig, Germany) from 3500 to 1000 cm^{-1} using an ATR diamond crystal.

Thermogravimetric Analysis. TGA was conducted on a Mettler Toledo (DSC-H22) instrument. The sample was heated in a platinum pan under a nitrogen atmosphere over a temperature range of 25−800 °C with a heating rate of 10 K min^{-1}.

Hybrid GUV Formation. The formation of DPPC/PIB_{87}-*b*-PEO_{17} BCP hybrid GUVs with incorporated PIB-functionalized CdSe NPs (**NP6**) was achieved as described previously[38] using an electroformation method originally reported by Angelova *et al.*[55] Water that was used for the study was purified *via* passage through a filtering system by Purelab Option system (ELGA Ltd., Celle, Germany), yielding ultrapure water. Briefly, all lipid/polymer mixtures varying in their compositions were additionally mixed with **NP6** using a NP to BCP ratio of 1 to 1500. The lipid/polymer mixtures containing **NP6** were prepared in chloroform (HPLC grade, Sigma Aldrich, Schnelldorf, Germany), dried under a continuous N_2-stream, and dissolved in a defined solvent volume, reaching a total concentration of 10 mg/mL. The final mixtures were used to generate a homogeneous thin film on optically transparent indium−tin-oxide (ITO)-coated coverslips (electrodes) *via* a spin-coating method. Afterward, the coverslips were placed in a capacitor-type configuration at a distance of 2 mm using a home-built flow-chamber. Finally, the flow-chamber was filled with water and the electroformation process started as reported previously.[38]

Giant Vesicle Analysis by Confocal Laser Scanning Microscopy. Confocal microscopy images were obtained on a commercially available confocal laser scanning microscope (LSM 710/ConfoCor 3; Carl-Zeiss, Germany) using a C-Apochromat 40×/1.2 NA water immersion objective. The hydrophobically functionalized NPs, which were fluorescently labeled with rhodamine B (**NP6**), were excited with a DPSS laser at 561 nm. All GUV imaging studies, monitoring the incorporation of CdSe NPs into hybrid GUVs in the case of either a mixed or phase-separated membrane morphology, were performed after cooling to room temperature (20 °C).

Synthesis of Polymer-Covered CdSe Nanoparticles (NP3, NP4, and NP5). Trioctylphosphine oxide-covered CdSe NPs (**NP1**) were synthesized by the conventional hot injection method according to ref 44. Ligand exchange of the relatively stable passivating TOPO on the CdSe nanoparticle surface with polymers **1**, **3**, and **4**, whose synthesis has been reported elsewhere,[57] was conducted according to Emrick *et al.*[58] as follows, yielding the nanoparticles **NP3**, **NP4**, and **NP5**, respectively. The TOPO ligand in **NP1** was replaced with a relatively weak pyridine ligand in other to facilitate the ligand exchange, and the pyridine-covered CdSe nanoparticles **NP2** (50 mg) were subsequently treated with α-phosphineoxide-γ-bromo telechelic polyisobutylene (**1**) PO-PIB_{57}-Br ($M_{n(GPC)}$ = 3200 g/mol; M_w/M_n = 1.3) (273 mg, 0.000 086 mmol) for hydrophobic PIB-covered CdSe nanoparticle (**NP3**). The hydrophilic water-soluble PEO-covered CdSe nanoparticle (**NP4**) and amphiphilic PIB_{57}-*b*-PEO_{12}-covered CdSe nanoparticle (**NP5**) were synthesized in a similar manner using α-phosphineoxide-γ-methylene telechelic PEO (**3**) PO-PEO_{47} (180 mg, 0.000 086 mmol) and α-phosphineoxide-γ-polyethylene oxide telechelic polyisobutylene (**4**) PO-PIB_{57}-*b*-PEO_{12} (292 mg, 0.000 086 mmol), respectively. The nanoparticles were dissolved in 10 mL of freshly distilled anhydrous toluene. The resulting mixture was stirred for 48 h at 70 °C. Toluene was evaporated under reduced pressure, and the polymer-covered NPs (**NP3**, **NP4**, and **NP5**) were precipitated three times in 20 mL of hexane followed by centrifugation to separate the free unbound polymer from the polymer-covered nanoparticles.

Synthesis of Polymer-Covered and Rhodamine-B-Labeled CdSe Nanoparticles (NP6). In order to easily locate hydrophobic PIB-covered CdSe NPs (**NP3**) in the DPPC:PIB_{87}-*b*-PEO_{17} mixed monolayer at the air/water interface using fluorescence spectroscopy, NPs were labeled with rhodamine-B as follows: a 80 to 20 wt % mixture of ligand **1** and **2** was dissolved in toluene and subsequently added to 50 mg of **NP2**. The mixture was heated at 70 °C for 48 h. Toluene was evaporated under reduced pressure, and the rhodamine-B-labeled NPs (**NP6**) were precipitated three times in 20 mL of hexane followed by centrifugation to separate the free polymer from the polymer-covered nanoparticle.

Conflict of Interest: The authors declare no competing financial interest.

Acknowledgment. We are grateful for the grant DFG BI 1337/6-1 (A.O., M.S.) within the Forschergruppe FOR-1145, the DFG grant within the Transregio-SFB TRR 102 (W.H.B., J.K.), and the grants DFG INST 271/249-1; INST 271/247-1; INST 271/248-1; and BMBF FKZ 03Z2HN22 (K.B.), which supported this work.

Supporting Information Available: Absorption and emission spectra of **2**, **NP1**, **NP3**, **NP4**, and **NP6**, ^{1}H NMR and IR spectra of **1**, **2**, **3**, and **4** with **NP3**, **NP4**, and **NP5**, AFM height image of **NP3** transferred at different surface pressure, and AFM height image of mixed DPPC:PIB_{87}-*b*-PEO_{17} in the ratios 60:40 and 80:20 mol % with and without nanoparticles are available free of charge *via* the Internet at http://pubs.acs.org.

REFERENCES AND NOTES

1. Binder, W. H.; Sachsenhofer, R.; Farnik, D.; Blaas, D. Guiding the Location of Nanoparticles into Vesicular Structures: A Morphological Study. *Phys. Chem. Chem. Phys.* **2007**, *9*, 6435–6441.
2. Gopalakrishnan, G.; Danelon, C.; Izewska, P.; Prummer, M.; Yves Bolinger, P.; Geissbhler, I.; Demurtas, D.; Dubochet, J.; Vogel, H. Multifunctional Lipid/Quantum Dot Hybrid

Nanocontainers for Controlled Targeting of Live Cells. *Angew. Chem., Int. Ed.* **2006**, *45*, 5478–5483.
3. Bothun, G. D. Hydrophobic Silver Nanoparticles Trapped in Lipid Bilayers: Size Distribution, Bilayer Phase Behavior, and Optical Properties. *J. Nanobiotechnol.* **2008**, *6*, 13–23.
4. Zhang, L.; Hong, L.; Yu, Y.; Bae, S. C.; Granick, S. Nanoparticle-Assisted Surface Immobilization of Phospholipid Liposomes. *J. Am. Chem. Soc.* **2006**, *128*, 9026–9027.
5. Haryono, A.; Binder, W. H. Controlled Arrangement of Nanoparticle Arrays in Block-Copolymer Domains. *Small* **2006**, *2*, 600–611.
6. Schulz, M.; Olubummo, A.; Binder, W. H. Beyond the Lipid-Bilayer: Interaction of Polymers and Nanoparticles with Membranes. *Soft Matter* **2012**, *8*, 4849–4864.
7. Li, N.; Binder, W. H. Click-Chemistry for Nanoparticle-Modification. *J. Mater. Chem.* **2011**, *21*, 16717–16734.
8. Barenholz, Y. Liposome Application: Problems and Prospects. *Curr. Opin. Colloid Interface Sci.* **2001**, *6*, 66–77.
9. Discher, D. E.; Eisenberg, A. Polymer Vesicles. *Science* **2002**, *297*, 967–973.
10. Binder, W. H.; Barragan, V.; Menger, F. M. Domains and Rafts in Lipid Membranes. *Angew. Chem., Int. Ed.* **2003**, *42*, 5802–5827.
11. Discher, D. E.; Ahmed, F. Polymersomes. *Annu. Rev. Biomed. Eng.* **2006**, *8*, 323–341.
12. Egli, S.; Nussbaumer, M. G.; Balasubramanian, V.; Chami, M.; Bruns, N.; Palivan, C.; Meier, W. Biocompatible Functionalization of Polymersome Surfaces: A New Approach to Surface Immobilization and Cell Targeting Using Polymersomes. *J. Am. Chem. Soc.* **2011**, *133*, 4476–4483.
13. Ginzburg, V. V.; Balijepalli, S. Modeling the Thermodynamics of the Interaction of Nanoparticles with Cell Membranes. *Nano Lett.* **2007**, *7*, 3716–3722.
14. Alexeev, A.; Uspal, W. E.; Balazs, A. C. Harnessing Janus Nanoparticles to Create Controllable Pores in Membranes. *ACS Nano* **2008**, *2*, 1117–1122.
15. Rozenberg, B. A.; Tenne, R. Polymer-Assisted Fabrication of Nanoparticles and Nanocomposites. *Prog. Polym. Sci.* **2008**, *33*, 40–112.
16. Chen, Y.; Bothun, G. D. Lipid-Assisted Formation and Dispersion of Aqueous and Bilayer-Embedded Nano-C60. *Langmuir* **2009**, *25*, 4875–4879.
17. Jeng, U. S.; Hsu, C. H.; Lin, T. L.; Wu, C. M.; Chen, H. L.; Tai, L. A.; Hwang, K. C. Dispersion of Fullerenes in Phospholipid Bilayers and the Subsequent Phase Changes in the Host Bilayers. *Phys. B (Amsterdam, Neth.)* **2005**, *357*, 193–198.
18. Park, S.-H.; Oh, S.-G.; Mun, J.-Y.; Han, S.-S. Loading of Gold Nanoparticles Inside the DPPC Bilayers of Liposome and their Effects on Membrane Fluidities. *Colloids Surf., B* **2006**, *48*, 112–118.
19. Bothun, G. D. Hydrophobic Silver Nanoparticles Trapped in Lipid Bilayers: Size Distribution, Bilayer Phase Behavior, and Optical Properties. *J. Nanobiotechnol.* **2008**, *6*, 13–23.
20. Park, S.-H.; Oh, S.-G.; Mun, J.-Y.; Han, S.-S. Effects of Silver Nanoparticles on the Fluidity of Bilayer in Phospholipid Liposome. *Colloids Surf., B* **2005**, *44*, 117–122.
21. El Rassy, H.; Belamie, E.; Livage, J.; Coradin, T. Onion Phases as Biomimetic Confined Media for Silica Nanoparticle Growth. *Langmuir* **2005**, *21*, 8584–8587.
22. Bothun, G. D.; Rabideau, A. E.; Stoner, M. A. Hepatoma Cell Uptake of Cationic Multifluorescent Quantum Dot Liposomes. *J. Phys. Chem. B* **2009**, *113*, 7725–7728.
23. Al-Jamal, W. T.; Al-Jamal, K. T.; Bomans, P. H.; Frederik, P. M.; Kostarelos, K. Functionalized-Quantum Dot Liposome Hybrids as Multimodal Nanoparticles for Cancer. *Small* **2008**, *4*, 1406–1415.
24. Al-Jamal, W. T.; Al-Jamal, K. T.; Tian, B.; Lacerda, L.; Bomans, P. H.; Frederik, P. M.; Kostarelos, K. Lipid-Quantum Dot Bilayer Vesicles Enhance Tumor Cell Uptake and Retention *in Vitro* and *in Vivo*. *ACS Nano* **2008**, *2*, 408–418.
25. Rasch, M. R.; Rossinyol, E.; Korgel, B. A.; Hueso, J. L.; Goodfellow, B. W.; Arbiol, J. Hydrophobic Gold Nanoparticle Self-Assembly with Phosphatidylcholine Lipid: Membrane Loaded and Janus Vesicles. *Nano Lett.* **2010**, *10*, 3733–3739.
26. Chen, Y.; Bose, A.; Bothun, G. D. Controlled Release from Bilayer Decorated Magnetoliposomes *via* Electromagnetic Heating. *ACS Nano* **2010**, *4*, 3215–3221.
27. Jing, B.; Zhu, Y. E. Disruption of Supported Lipid Bilayers by Semi-Hydrophobic Nanoparticles. *J. Am. Chem. Soc.* **2011**, *133*, 10983–10989.
28. Lipowsky, R.; Döbereiner, H. G. Vesicles in Contact with Nanoparticles and Colloids. *Europhys. Lett.* **1998**, *43*, 219–225.
29. Breidenich, M.; Netz, R. R.; Lipowsky, R. The Influence of Non-Anchored Polymers on the Curvature of Vesicles. *Mol. Phys.* **2005**, *103*, 3169–3183.
30. Noguchi, H.; Takasu, M. Adhesion of Nanoparticles to Vesicles: A Brownian Dynamics Simulation. *Biophys. J.* **2002**, *83*, 299–308.
31. Lin, Y.; Boker, A.; He, J.; Sill, K.; Xiang, H.; Abetz, C.; Li, X.; Wang, J.; Emrick, T.; Long, S.; *et al*. Self-Directed Self-Assembly of Nanoparticle/Copolymer Mixtures. *Nature* **2005**, *434*, 55–59.
32. Sanchez-Gaytan, B. L.; Cui, W.; Kim, Y.; Mendez-Polanco, M. A.; Duncan, T. V.; Fryd, M.; Wayland, B. B.; Park, S. Interfacial Assembly of Nanoparticles in Discrete Block-Copolymer Aggregates. *Angew. Chem., Int. Ed.* **2007**, *119*, 9395–9398.
33. Hickey, R. J.; Sanchez-Gaytan, B. L.; Cui, W.; Composto, R. J.; Fryd, M.; Bradford, B. W.; Park, J. Morphological Transitions of Block-Copolymer Bilayers *via* Nanoparticle Clustering. *Small* **2010**, *6*, 48–51.
34. Hickey, R. J.; Haynes, A. S.; Kikkawa, J. M.; Park, S. Controlling the Self-Assembly Structure of Magnetic Nanoparticles and Amphiphilic Block-Copolymers: From Micelles to Vesicles. *J. Am. Chem. Soc.* **2011**, *133*, 1517–1525.
35. Mai, Y.; Eisenberg, A. Controlled Incorporation of Particles into the Central Portion of Vesicle Walls. *J. Am. Chem. Soc.* **2010**, *132*, 10078–10084.
36. Lecommandoux, S.; Sandre, O.; Chécot, F.; Perzynski, R. Smart Hybrid Magnetic Self-Assembled Micelles and Hollow Capsules. *Prog. Solid State Chem.* **2006**, *34*, 171–179.
37. Krack, M.; Hohenberg, H.; Weller, H.; Kornowski, A.; Förster, S.; Lindner, P. Nanoparticle-Loaded Magnetophoretic Vesicles. *J. Am. Chem. Soc.* **2008**, *130*, 7315–7320.
38. Schulz, M.; Glatte, D.; Meister, A.; Scholtysek, P.; Kerth, A.; Blume, A.; Bacia, K.; Binder, W. H. Hybrid Lipid/Polymer Giant Unilamellar Vesicles: Effects of Incorporated Biocompatible PIB-PEO Block Copolymers on Vesicle Properties. *Soft Matter* **2011**, *7*, 8100–8110.
39. Binder, W. H. Polymer-Induced Transient Pores in Lipid Membranes. *Angew. Chem., Int. Ed.* **2008**, *47*, 3092–3095.
40. Meier, W.; Ruysschaert, T.; Sonnen, A. F. P.; Haefele, T.; Winterhalter, M.; Fournier, D. Hybrid Nanocapsules: Interactions of ABA Block Copolymers with Liposomes. *J. Am. Chem. Soc.* **2005**, *127*, 6242–6247.
41. Meier, W.; Kita-Tokarczyk, K.; Itel, F.; Grzelakowski, M.; Egli, S.; Rossbach, P. Monolayer Interactions between Lipids and Amphiphilic Block Copolymers. *Langmuir* **2009**, *25*, 9847–9856.
42. Nam, J.; Beales, P. A.; Vanderlick, T. K. Giant Phospholipid/Block Copolymer Hybrid Vesicles: Mixing Behavior and Domain Formation. *Langmuir* **2011**, *27*, 1–6.
43. Chemin, M.; Brun, P.-M.; Lecommandoux, S.; Sandre, O.; Le Meins, J.-F. Hybrid Polymer/Lipid Vesicles: Fine Control of the Lipid and Polymer Distribution in the Binary Membrane. *Soft Matter* **2012**, *8*, 2867–2874.
44. Binder, W. H.; Lomoschitz, M.; Friedbacher, G.; Sachsenhofer, R. Reversible and Irreversible Binding of Nanoparticles to Polymeric Surfaces. *J. Nanomater.* **2009**, ID 613813, doi: 10.1155/2009/613813.
45. Alivisatos, A. P. Semiconductor Clusters, Nanocrystals, and Quantum Dots. *Science* **1996**, *271*, 933–937.
46. Yu, W. W.; Qu, L.; Guo, W.; Peng, X. Experimental Determination of the Extinction Coefficient of CdTe, CdSe, and CdS Nanocrystals. *Chem. Mater.* **2003**, *15*, 2854–2860.
47. Li, H. H.; Yabuuchi, N.; Meng, Y. S.; Kumar, S.; Breger, J.; Grey, C. P.; Shao-Horn, Y. Changes in the Cation Ordering of Layered O3 $Li_xNi_{0.5}Mn_{0.5}O_2$ During Electrochemical Cycling

to High Voltages: An Electron Diffraction Study. *Chem. Mater.* **2007**, *19*, 2551–2565.
48. Ji, X.; Copenhaver, D.; Sichmeller, C.; Peng, X. Ligand Bonding and Dynamics on Colloidal Nanocrystals at Room Temperature: The Case of Alkylamines on CdSe Nanocrystals. *J. Am. Chem. Soc.* **2008**, *130*, 5726–5735.
49. Sachleben, J. R.; Wooten, E. W.; Emsley, L.; Pines, A.; Colvin, V. L.; Alivisatos, A. P. NMR Studies of the Surface Structure and Dynamics of Semiconductor Nanocrystals. *Chem. Phys. Lett.* **1992**, *198*, 431–436.
50. Cotton, F. A.; Barnes, R. D.; Bannister, E. The Effect of Complex-Formation by Phosphine Oxides on Their P-O Stretching Frequencies. *J. Chem. Soc. (Resumed)* **1960**, 2199–2203.
51. Sunday, D.; Curras-Medina, S.; Green, D. L. Impact of Initiator Spacer Length on Grafting Polystyrene from Silica Nanoparticles. *Macromolecules* **2010**, *43*, 4871–4878.
52. Ma, G.; Allen, H. C. DPPC Langmuir Monolayer at the Air-Water Interface: Probing the Tail and Head Groups by Vibrational Sum Frequency Generation Spectroscopy. *Langmuir* **2006**, *22*, 5341–5349.
53. El Kirat, K.; Besson, F.; Prigent, A.-F.; Chauvet, J.-P.; Roux, B. Role of Calcium and Membrane Organization on Phospholipase D Localization and Activity. *J. Biol. Chem.* **2002**, *277*, 21231–21236.
54. Li, H.; Sachsenhofer, R.; Binder, W. H.; Henze, T.; Thurn-Albrecht, T.; Busse, K.; Kressler, J. Hierarchical Organization of Poly(ethylene oxide)-Block-Poly(isobutylene) and Hydrophobically Modified Fe_2O_3 Nanoparticles at the Air/Water Interface and on Solid Supports. *Langmuir* **2009**, *25*, 8320–8329.
55. Angelova, M. I.; Dimitrov, D. S. Liposome Electroformation. *Faraday Discuss. Chem. Soc.* **1986**, *81*, 303–311.
56. Nam, J.; Vanderlick, T. K.; Beales, P. A. Formation and Dissolution of Phospholipid Domains with Varying Textures in Hybrid Lipo-Polymersomes. *Soft Matter* **2012**, *8*, 3982–3988.
57. Adekunle, O.; Herbst, F.; Hackethal, K.; Binder, W. H. Synthesis of Nonsymmetric Chain end Functionalized Polyisobutylenes. *J. Polym. Sci., Part A: Polym. Chem.* **2011**, *49*, 2931–2940.
58. Skaff, H.; Ilker, M. F.; Coughlin, E. B.; Emrick, T. Preparation of Cadmium Selenide−Polyolefin Composites from Functional Phosphine Oxides and Ruthenium-Based Metathesis. *J. Am. Chem. Soc.* **2002**, *124*, 5729–5733.